High-Throughput Protein Structural Analysis Using Site-Directed Fluorescence Labeling and the Bimane Derivative (2-Pyridyl)dithiobimane†

Steven E. Mansoor and David L. Farrens*

Department of Biochemistry and Molecular Biology, Oregon Health and Science University, 3181 SW Sam Jackson Park Road, Portland, Oregon 97239-3098

Received December 16, 2003; Revised Manuscript Received April 30, 2004

ABSTRACT: We present a site-directed fluorescence labeling (SDFL) study of 25 different T4 lysozyme protein samples labeled with the thiol-cleavable fluorophore, (2-pyridyl)dithiobimane (PDT-Bimane). Our results demonstrate PDT-Bimane can be used in cysteine-scanning studies to detect protein secondary structure, and to map proximity between sites in proteins by monitoring tryptophan quenching of bimane fluorescence. In addition, the reducible nature of PDT-Bimane can be exploited to resolve problems often faced in SDFL studies: ensuring specific labeling of cysteine residues, determining the extent of free label contamination, and accurately determining labeling efficiency even at low concentrations. The ability to cleave PDT-Bimane off the protein enables rapid determination of these parameters, and positions it as an ideal fluorophore for automated, high-throughput structural studies of protein folding, the detection of protein−protein interactions, and the monitoring of real-time conformational changes.

The ability to carry out site-directed fluorescence labeling (SDFL)[1] has dramatically advanced the type of questions biochemists can address using fluorescence spectroscopy (*1*−*12*). In brief, SDFL involves introducing unique cysteine residues at defined sites in a protein, then attaching fluorescent labels to these sites to act as local reporter groups. The information these probes report on their local environment (for example, buried vs solvent exposed) is then used to assess the structure and monitor dynamic changes in the protein. By systematically scanning through a protein region, SDFL can be used to obtain localized secondary structure information (*3*), map proximity in proteins (*10*), study protein folding (*13*), assess conformational changes in a protein's structure (*6*, *14*), determine membrane protein topology and insertion (*15*), and monitor protein−protein interactions (*16*). Similar information can be obtained using other site-directed methods, such as site-directed tryptophan fluorescence (*17*−*20*) or site-directed spin labeling (SDSL) (*21*−*31*).

Although powerful, SDFL is an immature structural technique still under development. To help standardize and improve our SDFL methods, we have been carrying out a series of scanning SDFL studies on the protein T4 lysozyme (T4L) (*3*, *10*), inspired by previous studies using SDSL (*32*−*37*). Our work has focused on using the small fluorescent probe monobromobimane (mBBr; Figure 1A) with the goal of defining exactly what structural information can be obtained in SDFL studies using this probe, and assessing the effect of introducing this fluorescent reporter group on the protein's structure and stability.

In the present paper, we report that our SDFL studies can be substantially improved and simplified by using a new bimane derivative, (2-pyridyl)dithiobimane (PDT-Bimane; Figure 1B). PDT-Bimane is small, and its unique properties provide key features that should allow automation of SDFL procedures. We demonstrate from scanning SDFL studies of 25 different T4L mutants (Figure 1C) that PDT-Bimane can be used to map solvent accessibility and determine local regions of protein secondary structure (by assessing shifts in the probe's emission λ_{max} values and changes in the steady-state anisotropy values). Further, we find PDT-Bimane fluorescence is dramatically quenched by proximal tryptophan residues, and this distance-dependent quenching can be used to obtain localized tertiary structure information.

A major goal of this paper is to develop procedures that substantially simplify SDFL studies of protein structure. We ultimately hope to combine these methods with the recently developed automated protein expression and purification systems (*38*), thus enabling automated, high-throughput studies of protein structure by SDFL methods.

We find that along with the well-established properties of bimane fluorescence, PDT-Bimane provides a key advantage for automating SDFL studies − it attaches to proteins through a reversible disulfide linkage. We find the nature of this linkage can be used to overcome a number of practical difficulties: ensuring label specificity and quantitating the amount of specific label incorporation into samples at low concentrations. Furthermore, the cleavable nature of PDT-Bimane can be exploited to dramatically simplify SDFL

† This work was supported by Grant EY12095 and Grant DA14896 to D.L.F. from the National Eye Institute and Grant F30DA15584 to S.E.M. from the National Institute of Drug Abuse.

* To whom correspondence should be addressed: Telephone: (503) 494-0583; fax: (503) 494-8393; e-mail: farrensd@ohsu.edu.

[1] Abbreviations: mBBr, monobromobimane; -B_1, protein sample labeled with mBBr; PDT-Bimane, (2-pyridyl)dithiobimane; -B_2, protein sample labeled with PDT-Bimane; Cys-B_2, PDT-Bimane reacted with L-cysteine; SDFL; site-directed fluorescence labeling; TCEP−HCl, Tris (2-carboxyethyl)phosphine hydrochloride; T4L, T4 lysozyme; Trp, tryptophan; Phe, phenylalanine; MOPS, 3-(*N*-morpholino)-propanesulfonic acid; Tris, 2-amino-2-(hydroxymethyl)-1,3-propanediol; EDTA, *N*,*N*′-1,2-ethanediylbis[*N*-(carboxymethyl)glycine]; SEM, standard error of the mean; PET, photoinduced electron transfer.

10.1021/bi036259m CCC: $27.50
Published on Web 07/01/2004

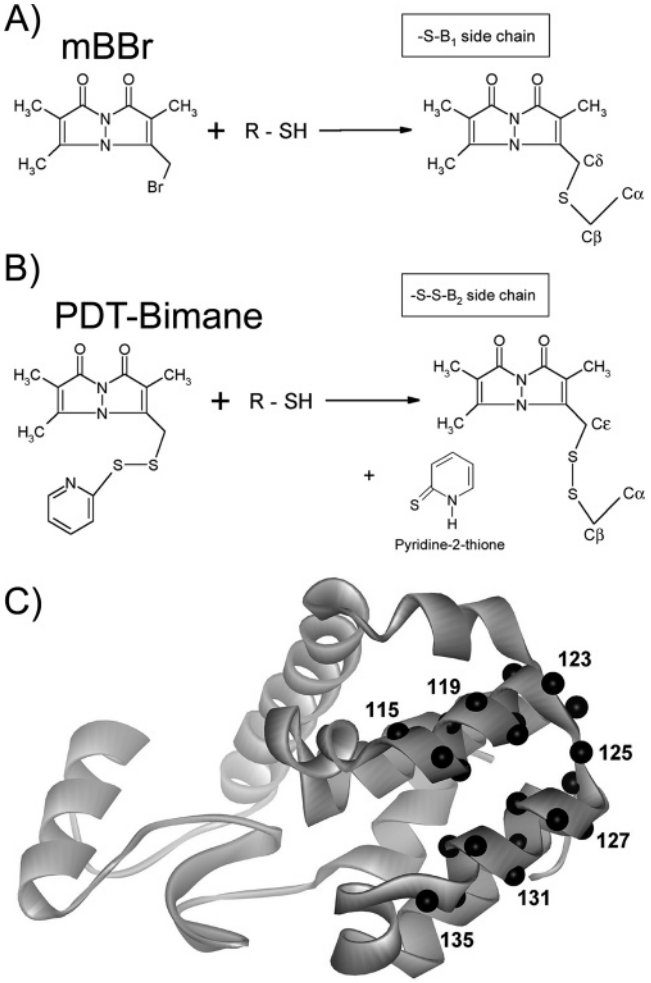

FIGURE 1: Reaction schemes for two bimane derivatives with sulfhydryl groups. (A) Reaction of the monobromobimane (mBBr) label with a sulfhydryl group to produce an -S-Bimane side chain ($-B_1$). (B) Reaction of the (2-pyridyl)dithiobimane (PDT-Bimane) label with a sulfhydryl group to produce an -S−S-Bimane side chain ($-B_2$). The latter reaction also results in the release of pyridyl-2-thione, which can be spectroscopically monitored at 343 nm (*39*). (C) Model of T4 lysozyme indicating sites of cysteine substitutions for the SDFL studies using PDT-Bimane. The black balls show the relative positions of each α-carbon substituted with a cysteine.

studies: by simply comparing spectra of labeled samples before and after reduction, one can rapidly assess the solvent accessibility (and thus secondary structure) of the region under study, and detect the proximity of the site to Trp residues.

In summary, the unique spectral properties of PDT-Bimane coupled with its ability to be reduced off proteins make it an ideal probe for automated, high-throughput SDFL studies of protein structure and function, for mapping protein−protein interactions, and for monitoring real-time conformational changes in proteins.

EXPERIMENTAL PROCEDURES

Materials. (2-Pyridyl)dithiobimane (PDT-Bimane or suffix $-B_2$) was purchased from Toronto Research Biochemicals. TCEP−HCl was purchased from Pierce. Quinine sulfate monohydrate was purchased from Aldrich Chemical Co. Neutral density filters, long-pass filters, and interference filters were from Oriel Corporation. All cuvettes were from Uvonics. All buffer components were purchased from Fisher-Biotech and GibcoBRL. The cysteine-free lysozyme gene (containing the substitutions C54T and C97A) was kindly provided by F. W. Dahlquist (University of Oregon). This will hereafter be called the "wild type" or T4L.

The buffers used were as follows: buffer A, 50 mM MOPS, 50 mM Tris, 1 mM EDTA, pH 7.6. Buffer B, 0.1 M Tris−HCl, 0.1 M Na_2EDTA. Buffer C, 20 mM Tris−HCl, 1 mM $CaCl_2$, pH 8.0. Buffer D, 20 mM Tris, 20 mM MOPS, 0.02% sodium azide, 1 mM EDTA, 1 mM DTT, pH 7.6. Buffer E, 20 mM KH_2PO_4, 25 mM KCl, pH 3.0. Buffer F, 50 mM MOPS, 50 mM Tris, 1 mM EDTA, pH 7.6, 3 M guanidine hydrochloride.

Construction, Expression, and Purification of Mutants. The construction and expression of the cysteine mutants used in the present work has been previously described in detail (*3*, *10*). Briefly, K38 *Escherichia coli* cells were transformed with the T4L cysteine-mutant plasmid, and protein production was induced in log-phase cultures, harvested, lysed in buffer D by French press, and clarified by centrifugation. Following centrifugation, the cell solution was filtered and DTT was added to 20 mM. After 30 min, the solution was loaded onto a Pharmacia Biotech HiTrap cation exchange column equilibrated with buffer A. The samples were eluted with a salt gradient (ramped from 0 to 1 M in 20 min). The purity of the proteins was assessed by SDS−PAGE and judged to be at least 90% pure for all samples studied.

Fluorescence Labeling. Labeling of each lysozyme mutant was carried out essentially as described previously (*3*, *10*) using a 5−10× molar excess of the fluorescent label in buffer F at 4 °C overnight. Free label was separated from labeled protein using gel filtration on a Pharmacia Biotech HiTrap desalting column previously equilibrated with buffer A and the labeling efficiency for each mutant was calculated from the absorption spectrum (using a Shimadzu UV 1601 UV−Vis spectrophotometer). Protein concentrations were calculated using an extinction coefficient of $\epsilon_{280} = 23\,327$ L cm^{-1} mole^{-1} for T4 lysozyme. A value of 5000 L cm^{-1} mol^{-1} was used for the PDT-Bimane label. Note that this value is based on the value of mBBr. A value of $\epsilon_{280} = 5600$ L cm^{-1} mol^{-1} was either added or subtracted to the WT T4 lysozyme extinction coefficient to correct for mutants that had a tryptophan introduced or removed, respectively. The contribution from the PDT-Bimane label at 280 nm was subtracted before calculating the protein concentrations. Control experiments using the cysteine-less WT protein showed that background labeling was less than 3% for PDT-Bimane (as judged by absorbance).

Monitoring Reaction Rate of PDT-Bimane. Reaction rates for PDT-Bimane can be determined by monitoring the formation of pyridine-2-thione (absorbance extinction coefficient $\epsilon_{343} = 8080$ L cm^{-1} mol^{-1}), the leaving group in the reaction of PDT-Bimane with a cysteine (see Figure 1B; *39*). The relative stability of the PDT-Bimane label in solution was assessed by monitoring the absorbance increase at 343 nm (as a function of time) from a 30 μM sample in buffer A (pH 7.6) and room temperature using a Shimadzu UV 1601 UV−Vis spectrophotometer. The resulting curve was fit to a single-exponential rise to maximum function in Sigma Plot 8.0 to give the rate of spontaneous hydrolysis.

The reaction rate of PDT-Bimane to a protein sample was performed by adding 12 μM of sample K124C (500 μL in buffer A) to a cuvette to which 5× molar PDT-Bimane was

rapidly mixed and monitored at room temperature for the formation of the pyridine-2-thione product (343 nm absorbance). The resulting curve was fit to a double exponential rise to maximum function with one of the rates being fixed at the rate obtained from the spontaneous hydrolysis experiment ($k = 4.4 \times 10^{-5}$ s^{-1}).

Nomenclature. The nomenclature for identifying the various mutations and bimane labeled T4 lysozyme derivatives follows the same formula as before (*3*, *10*). The samples are named by specifying the original residue, the number of the residue, and the new residue, in that order. For example, the code T115C indicates that the native threonine residue at the 115th amino acid position was mutated to a cysteine. Hereafter, protein samples labeled with a bimane fluorophore are indicated with the suffix -B_1 for mBBr, and -B_2 for PDT-Bimane. For example, the code T115B_2 indicates that the native threonine residue at the 115th amino acid position has been mutated to a cysteine and reacted with the PDT-Bimane label.

Protein Activity Assays. The enzymatic activity of each PDT-Bimane labeled mutant was measured by monitoring changes in light scattering due to the fluorescently labeled T4L digesting a suspension of peptidoglycan. As previously reported (*3*), the assay measured changes in light intensity at 365 nm (5-nm band-pass) from a 358 nm (1-nm band-pass) excitation beam using a Photon Technology International (PTI) steady-state fluorescence spectrophotometer. Reactions were initiated by adding 5 μL of PDT-Bimane labeled lysozyme mutants (2 μM in buffer A) to 350 μL of peptidoglycan solution, and the activity rates were determined from the initial slope of a plot of change in light intensity versus time. The mutants' activities thus determined are reported as a percentage of the wild type's activity. All measurements were performed in triplicate at 20 °C and the average values are reported.

Assessment of Thermodynamic Stability. A fluorescence assay (as previously described in refs *3* and *10*) was used to assess the thermodynamic stability and analyze the thermal unfolding properties of the PDT-Bimane labeled samples. Briefly, these measurements used 2 μM labeled protein (dialyzed against buffer E) and were measured using the PTI fluorometer in a T-format. Samples were excited at 280 nm and the fluorescence emission was monitored at 350 and 320 nm while the temperature was increased from 6 to 80 °C at a rate of 2 deg/min. At the end of each run, the samples were cooled back to 6 °C, to determine the extent of protein refolding, and melted again. Except for samples A130B_2, L133B_2, and A134B_2, the mutants showed greater than 75% refolding, as judged by the extent to which the ratio returned to its starting value. The reported T_m values are the average of the two melts thus measured and were calculated assuming a two-state model (native folded state and totally denatured state) in equilibrium. The $\Delta\Delta G$ values for each mutant were calculated using the approximation that $\Delta\Delta G = \Delta T_m \Delta S_{WT}$ (*40*) and the magnitude of these values were taken to reflect the amount of perturbation induced in the protein structure by the presence of the label. For more details, see ref *3*.

Solvent Sensitivity of Model Bimane Compounds. The sensitivity of PDT-Bimane fluorescence to solvent polarity was assessed by reacting PDT-Bimane with L-cysteine (5× excess) to create a model compound referred to as Cys-B_2. The Cys-B_2 model compound was then used to measure fluorescence emission spectra in dioxane/water mixtures ranging from 0 ($\epsilon = 79.5$) to 100% ($\epsilon = 2.2$) dioxane (v/v) at 22 °C. Wavelength maxima were determined from the first derivative of the spectra. The emission λ_{max} values thus obtained were used to generate a standard curve reflecting emission λ_{max} as a function of solvent dielectric (ϵ). This standard curve was subsequently used to assess the solvent polarity for each one of the PDT-Bimane labeled samples from T115−K135, based on their measured emission λ_{max} values. For more details, see ref *3*.

Steady-State Fluorescence and Anisotropy Measurements. All steady-state fluorescence excitation, emission, and anisotropy measurements were carried out using a PTI fluorescence spectrometer essentially as described previously (*3*, *10*). The fluorescence excitation measurements were carried out at 22 °C on 2 μM sample in buffer A and were measured from 300 to 450 nm using an integration time of 1 s, a step size of 1 nm, and a corrected emission signal at 490 nm. Excitation slits were 1-nm band-pass and emission slits were set at 15-nm band-pass. Fluorescence emission measurements to determine the emission λ_{max} values of the PDT-Bimane labeled mutants were taken at 22 °C, using 2 μM sample in buffer A and measured from 395 to 600 nm with excitation at 381 nm, using an integration time of 1 s, a step size of 1 nm, and a corrected emission signal. Excitation and emission slits were 10- and 1-nm band-pass, respectively.

All other emission measurements (i.e., for comparing fluorescence intensities of PDT-Bimane labeled samples with and without Trp residues) used samples at 5 μM in buffer A. These emission spectra were measured from 395 to 600 nm (1-nm band-pass) with excitation at 381 nm (3-nm band-pass), a 1-nm step size, and a 1 s integration time.

Anisotropy measurements were carried out at 15 °C using each PDT-Bimane labeled sample (2 μM) in buffer A. Excitation was at 381 nm (4-nm slits) and emission was collected at 475 nm (5-nm slits) with the samples lightly stirred. The measurements were performed in triplicate and the average steady-state anisotropy was obtained.

Quantum Yield Measurements. The quantum yields for the PDT-Bimane labeled mutants, as well as for PDT-Bimane, free in solution at pH 4.0, were measured using a Quinine Sulfate standard (quantum yield equal to 0.55 in 1 N H_2SO_4), as described previously (*3*, *10*). The quantum yields of 5 μM PDT-Bimane labeled protein samples in buffer A were measured using 360 nm excitation (3-nm band-pass) while monitoring emission from 370 to 700 nm (1-nm band-pass) and compared to the quinine sulfate standard measured under identical conditions. The buffer intensity was subtracted from all samples before integration from 370 to 625 nm. The quantum yield of the PDT-Bimane label, free in solution, was measured by first reacting a stock solution of the label with 15× TCEP−HCl (to remove the pyridyl group from the bimane moiety). The TCEP-reacted stock PDT-Bimane sample was then aliquoted into a 400 mM sodium acetate (pH 4.0) buffer to 5 μM, and emission scans were taken as described above. Using these conditions, the quantum yield of reduced PDT-Bimane at pH 4.0 was established to be 0.27.

Lifetime Measurements. All fluorescence lifetimes were measured at 22 °C using a PTI Laserstrobe fluorescence lifetime instrument on 250 μL of 5 μM samples (*3*, *10*, *41*).

Measurements used 381 nm excitation passed through a 298−435 nm band-pass filter, and emission was monitored through two long-pass filters (>470 nm). The instrument response function (IRF ~ 1.5 ns) was determined using a solution of Ludox. Each lifetime decay was measured using two averages of five shots per point, collected randomly in time over 150 channels. Data were acquired using an arithmetic data collection method, and analyzed using the commercial PTI T-Master software with either single exponential or double exponential fits. Goodness of fit was evaluated by χ^2 values (acceptable values between 0.8 and 1.2) and visual inspection of the residuals.

For data requiring a two-exponential analysis, the amplitude-weighted fluorescence lifetime, $\langle\tau\rangle = \alpha_1*\tau_1 + \alpha_2*\tau_2$, where α_1 and α_2 are the preexponential factors ($\alpha_1 + \alpha_2 = 1.0$) for τ_1 and τ_2, respectively, was used to represent the "average" lifetime for the sample. The value of the amplitude-weighted fluorescence lifetime represents the area under the decay curve and is thus proportional to the steady-state intensity (i.e., quantum yield) (*42*−*46*). This is easily shown in the following derivation, adapted from ref *46*.

The fluorescence decay is represented by the following sum of exponentials:

$$E(t) = \sum_{i=1}^{N} \alpha_i e^{-t/\tau_i}$$

where the sum of α_i is normalized to unity. The steady-state fluorescence intensity, (*I*), is proportional to the integral of $E(t)$:

$$I \propto \sum_{i=1}^{N} \alpha_i \int_0^\infty e^{-t/\tau_i} dt = \sum_{i=1}^{N} \alpha_i \tau_i$$

Thus, the steady-state intensity is proportional to the amplitude-weighted fluorescence lifetime. Deviations from this proportionality, for example, when changes in steady-state intensity are not reflected by comparable changes in the fluorescence decay, suggest underlying static quenching mechanisms are affecting the fluorescence of the fluorophore (*43*, *47*). In the discussion section, we show how identifying the type of quenching (i.e., dynamic quenching vs static quenching) can be used to determine the distance between the PDT-Bimane label and the Trp residue.

Calculation of Solvent-Accessible Surface Area. The solvent-accessible surface area for each residue between T115−K135 was calculated with the program ICM Lite (*48*) using a probe radius of 1.4 Å (radius of a water molecule) and the crystal structure coordinates of a cysteine-less WT T4 lysozyme mutant (PDB file 1L63; *49*).

Reduction and pH-Dependent Fluorescence Properties of Free, Reduced PDT-Bimane Label. To assess the pH dependence of the free, reduced fluorophore, PDT-Bimane (0.5 mM in buffer A) was reacted with the reducing agent TCEP (5× molar excess) for 20 min to produce −S-Bimane and pyridine-2-thione (see Figure 1B). This reaction mixture was then aliquoted to a 5 μM final concentration in sodium phosphate buffer varying from pH = 3.0 to pH = 10.0 to assess the pH-dependent titration of the remaining thiol on this bimane derivative. The fluorescence intensities of these reduced bimane samples were measured in the steady-state fluorometer by taking emission scans from 395 to 600 nm (1-nm band-pass) while exciting at 381 nm (3-nm band-pass).

Effect of Reducing PDT-Bimane Labeled Protein Samples on Fluorescence Intensity. The effect of reducing the PDT-Bimane label off the protein was assessed by adding 10 μL from a 100 mM TCEP−HCl stock to 200 μL of a 5 μM PDT-Bimane labeled sample in buffer A (absorbance of samples matched at 380 nm). Although it is not necessary to do so, the TCEP−HCl stocks were made up fresh before each set of experiments and used immediately. It has been shown that TCEP−HCl, in the absence of phosphate buffers (such as the buffers we used when reducing the label), is resistant to oxidation (<20%) at millimolar concentrations for periods up to 3 weeks, with no change in concentration detected after 24 h at room temperature (*50*). This reaction was allowed to proceed for 5 min and then 30 μL of 2.5 M sodium acetate (pH 4.0) was added to lower the pH to 4.0. Fluorescence emission scans were recorded before and after fluorophore reduction to monitor fluorescence intensity changes by exciting at 381 nm (3-nm band-pass) and averaging 2 emission scans from 395 to 700 nm (1-nm band-pass). The fluorescence intensity values obtained for each PDT-Bimane labeled sample were determined by the fraction of its integrated intensity from 370 to 700 nm as compared to the same sample with the fluorophore reduced (pH 4.0). Before integrating the total intensity from 370 to 700 nm, the dilution factors were accounted for and the buffer intensity was subtracted.

TCEP Reduction Method to Determine the Extent of PDT-Bimane Labeling and Extent of Free Label Contamination. A protocol for determining the amount of free label was developed that involves comparing the fluorescence intensities of the labeled protein samples before and after protein precipitation with TCA. The procedure was as follows. Two tubes containing 100 μL of sample at identical concentrations were first prepared. To tube I, 100 μL of 10% TCA was added. To tube 2, 100 μL of 100 mM TCEP was added. Both tubes were allowed to incubate at room temperature for 5 min and then spun for 5 min on a tabletop centrifuge. After centrifugation of the sample, 100 μL from each tube was removed and placed into fresh eppendorf tubes. To tube I, 100 μL of 100 mM TCEP was added and to tube II, 100 μL of 10% TCA was added. The fluorescence of each tube was then measured and compared using excitation at 381 nm (3-nm band-pass) and monitoring the fluorescence emission intensity from 395 to 600 nm (1-nm band-pass). Note that this protocol results in tube I and tube II receiving identical treatment but in a different order (see Figure 4A). Finally, note that the TCA precipitation protocol does not result in the precipitation of free PDT-Bimane label (data not shown).

To quantitate the total amount of label present on a protein sample, a standard curve of fluorescence intensity as a function of PDT-Bimane concentration was generated. Briefly, this first involved making PDT-Bimane stock solutions from 50 nM to 40 μM in 0.4 M sodium acetate (pH 4.0). To 200 μL each of these stock PDT-Bimane solutions, 10 μL of 100 mM TCEP was added (5-min incubation), followed by 190 μL of 10% TCA. The fluorescence intensity of each sample was measured using 381 nm excitation (3-nm band-pass) while collecting emission from 395 to 600 nm (1-nm band-pass). This generated a plot

Table 1: Characterization of PDT-Bimane Labeled T4 Lysozyme Mutants at Residues 115−135

mutant no.	mol label/ mol protein	activity (%WT)	ΔT_m[a] (°C)	$\Delta\Delta G$[b] (kcal/mol)
$T115B_2$	0.9	121	−3.4	−1.0
$N116B_2$	0.9	161	−1.6	−0.5
$S117B_2$	0.6	46	−1.0	−0.3
$L118B_2$	0.9	69	−8.9	−2.5
$R119B_2$	0.4	150	−3.9	−1.1
$M120B_2$	0.7	62	−5.8	−1.7
$L121B_2$	0.9	41	−14.1	−4.0
$Q122B_2$	0.6	100	−2.8	−0.8
$Q123B_2$	0.8	93	−3.5	−1.0
$K124B_2$	0.8	72	−4.7	−1.3
$R125B_2$	0.8	98	−3.5	−1.0
$W126B_2$	1.1	109	−13.8	−3.9
$D127B_2$	0.7	41	−4.3	−1.2
$E128B_2$	0.7	42	−3.4	−1.0
$A129B_2$	0.7	36	−11.3	−3.2
$A130B_2$	0.7	119	−6.4	−1.8
$V131B_2$	0.6	100	−1.5	−0.4
$N132B_2$	0.8	120	−0.2	−0.1
$L133B_2$	0.3	57	−10.4	−3.0
$A134B_2$	0.6	72	−0.2	−0.1
$K135B_2$	0.7	91	−4.7	−1.3

[a] T_m for wild-type T4L = 52.4 °C. [b] $\Delta\Delta G = \Delta T_m \Delta S_{wt}$ (ΔS_{wt} = 284.6 cal mol^{-1} K^{-1}).

of fluorescence intensity as a function of PDT-Bimane concentration. Following generation of the standard curve, 200 μL of a labeled protein sample was subjected to the same protocol (10 μL of 100 mM TCEP was added, followed by 190 μL of 10% TCA). The fluorescence intensity produced by the sample, following buffer subtraction, was compared to the standard curve to yield the concentration of bimane in the labeled protein sample.

RESULTS

Characterization of PDT-Bimane and Labeled Mutants. *Labeling Efficiency*. Table 1 reports the labeling efficiency of the mutants used in this study. This region of T4L was chosen since it possesses two significant stretches of secondary structure (a helix−turn−helix motif; see Figure 1C) and was previously studied with mBBr (*3*). Most of the samples could be labeled with efficiencies between 0.7 and 0.9, although interestingly, two of the sites, $R119B_2$ and $L133B_2$, displayed lower labeling efficiencies (0.4 and 0.3, respectively), even though the labeling was carried out on guanidine-denatured samples. We anticipate PDT-Bimane to be more selective for cysteine residues than other derivative bimane probes (such as monobromobimane and monochlorobimane) because it attaches to cysteines via a disulfide exchange reaction. In contrast, the monobromo- and monochlorobimanes attach to the most reactive nucleophile available through an S_N2 reaction usually, but not always, a cysteine at pH 7.4.

Stability of PDT-Bimane Free in Solution and Reaction Rate With Protein Samples. We find the spontaneous hydrolysis of a 30 μM solution of PDT-Bimane in buffer A (pH 7.6) is slow, but not insignificant, and occurs with a $\tau_{1/2}$ of about 4.5 h. In contrast, the rate of labeling of 12 μM mutant K124C in buffer A, using 60 μM PDT-Bimane, occurs with a $\tau_{1/2}$ of ~12 min. Thus, under these conditions, the rate of labeling the protein sample is >20× faster than the rate of spontaneous hydrolysis (data not shown).

Functional and Thermodynamic Assessments. Our functional studies showed that all the PDT-Bimane labeled samples retained some enzymatic activity, measured by their ability to breakdown a preparation of *E. coli* cell walls. In general, mutants where the label is incorporated at buried sites show substantially reduced activity, although this is not always the case (Table 1). Similarly, the thermodynamic stabilities of the PDT-Bimane labeled mutants (Table 1) indicate protein stability is generally impaired only for mutants whose labeled site is buried in the protein structure. We feel the thermodynamic stability data better reflect global structural perturbation due to the bimane label than do enzyme activity assays, since some residues may play a functional role as well as a structural one.

Spectral Properties of PDT-Bimane Reflect Solvent Accessibility at the Site of Attachment. The fluorescence of PDT-Bimane is solvent sensitive (Figure 2A), thus emission spectra of the PDT-Bimane labels attached to the protein at exposed sites (i.e., $K135B_2$) are more red-shifted than when attached at buried sites (i.e., $L133B_2$). We calibrated this sensitivity by reacting PDT-Bimane with L-cysteine and then measuring the fluorescence of this compound ($Cys\text{-}B_2$) in different mixtures of dioxane (dielectric, $\epsilon = 2.2$) and water (dielectric, $\epsilon = 79.5$). These measurements allowed us to generate an "apparent polarity" scale, which we used to compare with the PDT-Bimane labeled T4L samples. The advantage of this approach is that it provides an instrument-independent way to compare results. i.e., any systematic error in wavelength accuracy for a particular instrument is removed by measuring an apparent polarity scale using model compounds on the same instrument (*3*). Note that the "apparent polarity" thus determined for each site compares well with the solvent-accessible surface calculated from the crystal structure (Figure 2B).

As seen in the inset of Figure 2A, the emission λ_{max} values for $Cys\text{-}B_2$ vary as a function of the "apparent polarity". Two linear regions are observed, one from $\epsilon \sim 2$ to 10, and a second from $\epsilon \sim 18$ to 80. Fits to these linear regions yield the following relationships: $W = 2.02(\text{nm}/\epsilon)D + 432.7$ nm (for $\epsilon \sim 2$ to 10) and $W = 0.28$ (nm/ϵ)$D + 451.6$ nm (for $\epsilon \sim 18$ to 80), where W is the absorbance wavelength in nanometers and D is the dielectric constant (ϵ). Comparing these results with this region of the T4L structure (Figure 1C) indicates that emission λ_{max} values for the PDT-Bimane labeled samples reflect the solvent surface accessibilities of the residues from 115 to 135, as calculated from the crystal structure (Figure 2B).

Measurement of PDT Fluorophore Mobility. The steady-state fluorescence anisotropy values of PDT-Bimane labeled samples also reflect the solvent accessibility of the probes at the points of attachment. As expected, labels at buried sites reveal a higher steady-state anisotropy since their rotational mobility is restricted. There are, however, some outliers that may be related to differences in fluorescence lifetimes or because of local interactions between the label and the protein, both of which will affect the apparent steady-state anisotropy. The absolute values are given in Table 2 (to facilitate comparison with the solvent-accessible surface, the inverse of these anisotropy values are plotted in Figure 2C).

Power Series Calculation of SDFL Data Can Be Used to Assess Protein Secondary Structure. To provide a more

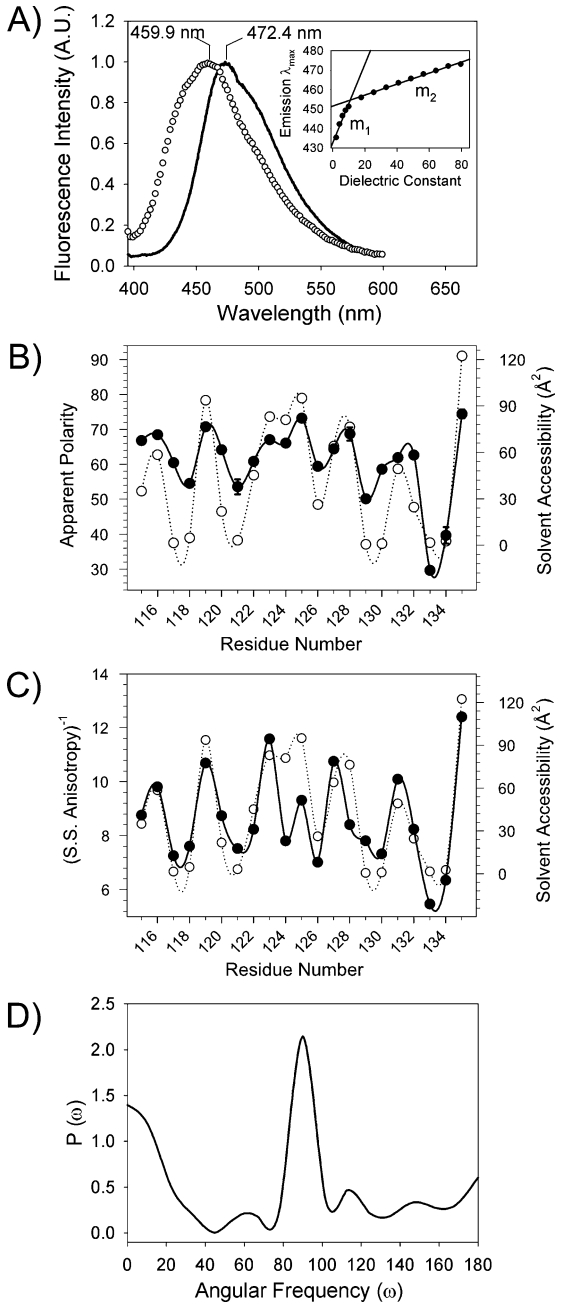

FIGURE 2: Scanning SDFL studies using PDT-Bimane can be used to map solvent accessibility and protein secondary structure. (A) The spectral properties of PDT-Bimane reflect the surrounding solvent polarity. The probe shows a blue-shift in fluorescence emission when attached to a buried site ($L133B_2$, open circles) in comparison to an exposed site ($K135B_2$, black line). The inset shows the emission λ_{max} of PDT-Bimane reacted with cysteine measured in solvents of different polarity. (B) Comparison of the apparent polarity determined for PDT-Bimane at each attachment site (black circles) with the solvent accessibility calculated from the T4 lysozyme crystal structure (open circles). (C) Comparison of the inverted steady-state fluorescence anisotropy values (black circles) with the calculated solvent accessibility (open circles). The fluorescence data in panels B and C represent measurements carried out in triplicate (note that the error bars in most cases are hidden by the symbols). In panels B and C, the solid black and dashed lines represent a cubic-spline fit of the respective data. (D) Fourier transform spectral density analysis of the normalized fluorescence emission apparent polarity values averaged with the normalized steady-state anisotropy values. Note the large peak at 96°, indicating the presence of an α-helix.

Table 2: Spectral Characterization of PDT-Bimane Labeled T4 Lysozyme Mutants at Residues 115−135

mutant no.	abs λ_{Max} (nm)	excitation[a] λ_{Max} (nm)	emission[b] λ_{Max} (nm)	steady-state anisotropy[c] ($\times 10^{-3}$)
$T115B_2$	386.7	389.0 ± 0.6	470.3 ± 0.2	114.1 ± 0.8
$N116B_2$	385.2	389.1 ± 1.0	470.8 ± 0.1	101.9 ± 0.5
$S117B_2$	382.0	388.5 ± 0.2	468.5 ± 0.2	137.8 ± 4.7
$L118B_2$	384.1	387.1 ± 0.2	466.9 ± 0.1	131.4 ± 3.6
$R119B_2$	387.6	388.5 ± 0.2	471.4 ± 0.2	93.5 ± 2.5
$M120B_2$	389.5	388.3 ± 0.6	469.6 ± 0.1	114.5 ± 11.1
$L121B_2$	389.3	388.4 ± 0.4	466.6 ± 0.6	132.9 ± 2.8
$Q122B_2$	391.3	388.2 ± 0.7	468.6 ± 0.1	121.4 ± 2.0
$Q123B_2$	394.7	389.8 ± 0.4	470.4 ± 0.1	86.3 ± 1.9
$K124B_2$	394.1	390.5 ± 0.3	470.1 ± 0.3	128.1 ± 6.8
$R125B_2$	391.6	383.9 ± 0.3	472.1 ± 0.2	107.4 ± 1.8
$W126B_2$	389.5	388.8 ± 0.6	468.2 ± 0.1	142.6 ± 2.9
$D127B_2$	387.8	389.0 ± 0.4	469.6 ± 0.1	93.0 ± 0.3
$E128B_2$	391.6	396.4 ± 0.1	470.8 ± 0.5	118.9 ± 0.8
$A129B_2$	384.2	387.5 ± 0.5	465.6 ± 0.1	128.0 ± 2.0
$A130B_2$	385.3	385.0 ± 0.4	468.0 ± 0.2	136.5 ± 2.4
$V131B_2$	374.3	382.6 ± 1.2	468.9 ± 0.1	99.1 ± 4.0
$N132B_2$	384.6	387.6 ± 0.1	469.1 ± 0.2	121.4 ± 3.6
$L133B_2$	383.7	383.4 ± 0.3	459.9 ± 0.1	183.0 ± 7.4
$A134B_2$	383.6	381.8 ± 1.2	462.7 ± 0.7	157.5 ± 5.8
$K135B_2$	391.0	391.4 ± 1.0	472.4 ± 0.3	80.6 ± 1.5

[a] Emission collected at 490 nm. [b] Excitation at 381 nm. [c] The uncertainty represents the SEM of three measurements.

quantitative comparison of the PDT-Bimane data with the solvent-accessible surface of T4L, we carried out a power series analysis of the periodicity in the emission λ_{max} data combined with the fluorescence anisotropy data (shown in Figure 2D). Note that the data shows good agreement with that expected for a region that is α-helical, exhibiting primarily periodicity of ~96°. Further details on the power series calculation are given in ref *3*.

Fluorescence Intensity of Reduced PDT-Bimane is pH Dependent, but PDT-Bimane Attached to the Protein Is Not. The PDT-Bimane label can be reduced off T4L, using TCEP as a reducing agent (see Figure 3A). However, when carrying out these studies, we found the fluorescence intensity of the resulting $^-$S-Bimane increases as the pH is lowered (Figure 3B), presumably as the resulting free thiol group becomes protonated. Titration of this effect shows an inflection point at approximately pH 6.5, a value within the range of possible pK_a's observed for thiol groups (Figure 3C). Identical results were obtained using β-mercaptoethanol as the reducing agent, indicating this effect is not TCEP dependent (data not shown). The fluorescence lifetime of TCEP reduced PDT-Bimane is also increased from $\tau = 6.2$ ns (pH 10.0) to $\tau = 10.4$ ns (pH 3.0) at the lower pH values (Figure 3D), consistent with an increase in quantum yield. Importantly, we find PDT-Bimane fluorescence is *not* pH dependent when attached to the protein (Figure 3E).

The fluorescence lifetime of PDT-Bimane is not mono-exponential, thus in this paper we report the amplitude-weighted fluorescence lifetime, $\langle\tau\rangle$, described by the formula $\langle\tau\rangle = \alpha_1\tau_1 + \alpha_2\tau_2$, where α_1 and α_2 are the normalized preexponential factors (i.e., $\alpha_1 + \alpha_2 = 1.0$) for each lifetime, τ_1 and τ_2, respectively. The amplitude-weighted fluorescence $\langle\tau\rangle$ lifetime is used here because it represents the area under the decay curve and thus, in the absence of static quenching phenomena, is proportional to the steady-state intensity (see Experimental Procedures for details).

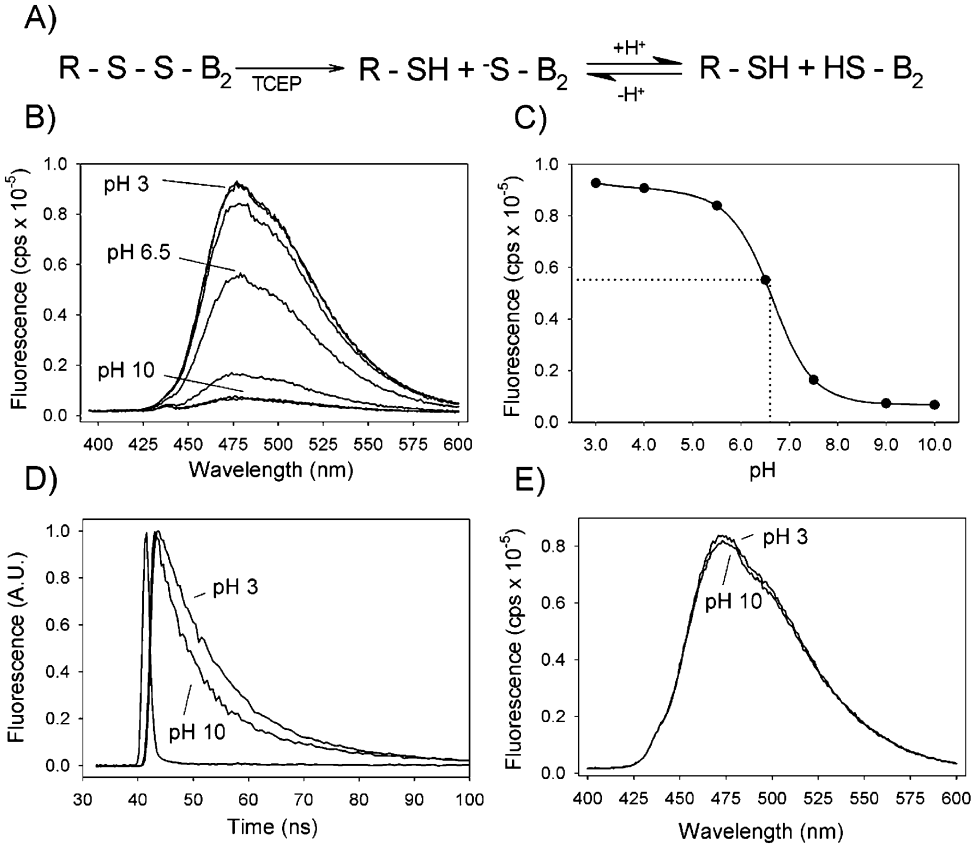

FIGURE 3: Reduced PDT-Bimane exhibits a strong pH dependence of fluorescence intensity. (A) The proposed chemical scheme for the Tris[2-carboxyethyl]-phosphine (TCEP) reduction of an R-S−S-B_2 labeled sample. Note that in this scheme, the reduced label can exist either as $^{-}$S-B_2 or HS-B_2, depending on the pH of the buffer. (B) Emission scans of TCEP reduced PDT-Bimane across the pH range 3.0 to 10.0. (C) Plot of maximum fluorescence intensity from panel B as a function of pH. Note the inflection point at pH 6.5, consistent with the protonation of the free thiol group produced by cleaving the disulfide. (D) Fluorescence lifetime decay curves of TCEP reduced PDT-Bimane exhibit an increase in fluorescence lifetime at pH 3.0 ($\langle\tau\rangle = 10.4$ ns) vs pH 10.0 ($\langle\tau\rangle = 6.2$ ns). (E) Emission scans of PDT-Bimane labeled protein samples at pH 3.0 vs pH 10.0. Note that the PDT-Bimane fluorescence is *not* sensitive to pH when the label is attached to a protein sample.

Labeling Efficiency and Specificity can be Determined using a Protocol Combining TCEP Reduction and TCA Protein Precipitation. We find TCEP reduction of PDT-Bimane can be used to determine both the total amount of bimane label and the amount of free, unattached label present in the sample. Importantly, this approach can even be used at low sample concentrations, which cannot be determined from absorbance spectra.

The protocol is as follows. The protein samples are first treated with TCA to precipitate the protein. Any fluorescence signal remaining in the supernatant after centrifugation is assumed to be free, unattached label. To determine the *total* amount of PDT-Bimane label present, the samples are first reduced with TCEP (as described above) *prior* to TCA precipitation and centrifugation. Finally, these two values are compared to standard curves of PDT-Bimane (generated by the same protocol as the samples) to determine the molar amounts of label present, from which the extent of specific protein labeling can then be calculated.

Figure 4 shows an example of this analysis carried out on sample N132B_2. Note that, after TCA precipitation, very little (<2.5%) of the total signal remains, indicating minimal free label contamination (Figure 4B). The labeling efficiency of this sample was next determined by subjecting the sample at concentration 1.2 μM (determined by absorbance) to the protocol described above. The results in Figure 4C show that a value of 1.1 μM PDT-Bimane was obtained from the standard curve, indicating this procedure can be used to reliably determine labeling efficiency.

PDT-Bimane Displays Distance Dependent Quenching by Proximal Tryptophan Residues, and the Quenching Is Removed Upon Reduction With TCEP. To test if proximal Trp residues quench PDT-Bimane fluorescence (as they do for mBBr) (*10*), we introduced a Trp residue at site 116 in T4L, and measured its effect on a PDT-Bimane probe introduced on nearby sites 123, 128, 132, and 135 (see Figure 5A). As expected, the Trp residue affects the fluorescence intensity of the PDT-Bimane labeled sites in a manner consistent with their relative proximity. For example, the bimane label at site 132, closest to W116, shows the largest amount of quenching (compare N132B_2 with N116W/N132B_2). In contrast, the bimane labels farthest away from site 116 (sites 123 and 135) show the least amount of quenching. The tryptophan-induced quenching is observed as an effect on both the steady-state fluorescence intensity (Figure 5B) and the fluorescence lifetimes (Table 3). Furthermore, we carried out an independent test of the Trp/bimane quenching hypothesis by measuring the effect of reducing the samples with TCEP. As seen in Figure 5C, addition of TCEP to reduce the PDT-Bimane off the samples

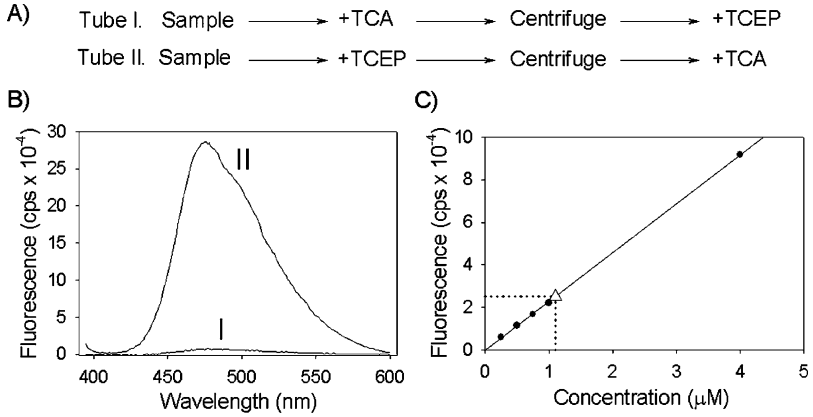

FIGURE 4: A protocol combining TCA precipitation and TCEP reduction can be used to reveal the presence of unreacted, free label in samples and to determine total labeling efficiency. (A) Protocol for determining presence of free, unreacted label (Tube 1), and for determining total labeling efficiency (Tube 2). (B) Spectrum I shows that TCA precipitation of samples followed by centrifugation and TCEP treatment results in essentially no fluorescence compared to the same sample that is first treated with TCEP before TCA precipitation and centrifugation (spectrum II), indicating there is no unattached, free label in the sample. (C) Example of determining labeling efficiency by comparing TCEP reduced samples to a standard curve of PDT-Bimane. The plot shows a sample of concentration 1.2 μM (determined by absorbance) subjected to the TCA/TCEP precipitation protocol, and compared to the standard curve. Notice that a value of 1.1 μM PDT-Bimane was obtained, indicating this procedure can be used to reliably determine labeling efficiency.

is accompanied by an increase in fluorescence, the magnitude of which depends on proximity to the Trp residue. These results are further analyzed in Discussion.

DISCUSSION

Overview. We set out to explore whether a new bimane derivative, PDT-Bimane, might prove advantageous for use in SDFL studies of protein structure. Our hope was this label could be used to determine localized regions of secondary structure and short-range distances within proteins, while also providing a unique ability to overcome problems that plague SDFL studies: (i) concern about labeling of noncysteine residues, (ii) problems with determining the molar labeling efficiency and extent of free label contamination, and (iii) circumventing the need to carry out the labor-intensive procedures such as matching sample concentrations for comparative studies. As discussed below, we find PDT-Bimane can be used to address all of these issues, and can greatly simplify the process of carrying out SDFL studies, potentially allowing for automation and high-throughput proteomic studies.

Advantages of PDT-Bimane for Preserving Protein Function and Stability and for Determining Labeling Efficiency. The function and thermodynamic stability of T4L are mainly affected only when the PDT-Bimane is introduced at buried sites (Table 1). We previously observed a similar result for mBBr, but the PDT-Bimane appears to be slightly less destabilizing than mBBr. One explanation may be the disulfide bond in PDT-Bimane allows additional degrees of rotational freedom, thus enabling the protein to undergo structural dynamics necessary for function and stability. This conclusion is consistent with previous analysis of EPR spin-label probes on T4L, which found nitroxide spin labels attached through a disulfide linkage increased the tolerance to the exogenous probe (*32*), because the disulfide bond allows the probe to alter its conformations to minimize steric clash at buried sites (*36*).

Another advantage of PDT-Bimane is that the ability to cleave it off the protein and compare it to standards provides a simple way to quantitate both labeling efficiency and the extent of free label contamination. This approach is very useful for samples with concentrations in the nanomolar range, which cannot be accurately measured on an absorbance spectrometer. Finally, because PDT-Bimane attaches to proteins through a disulfide bond, it specifically reacts with cysteine residues, as opposed to mBBr, which has the potential to label other amino acid residues under unusual circumstances (*51*).

PDT-Bimane Can be Used in Scanning SDFL Studies to Map the Solvent-Accessible Surface of a Protein and thus Determine Secondary Structure. Our results indicate that, in general, the emission λ_{max} and steady-state anisotropy values of PDT-Bimane labeled protein samples reliably report on the local environment around the probe. Thus, PDT-Bimane can be used in an SDFL scan to map the solvent-accessible surface of a protein by assessing the "apparent polarity" at each site and the mobility of the attached probe. Although visual inspection of these data (Figure 2B,C) can be used to glean the probable secondary structure of the region under study, a more quantitative result can be obtained by analyzing the results using a power series analysis that calculates periodicity in the data. For example, a strong periodic peak at ~96° indicates the region of the protein is an α-helix (Figure 2D), as would be expected.

PDT-Bimane Can be Used to Map Proximity Within Proteins Through Monitoring Trp Quenching of Bimane Fluorescence. As we previously found for mBBr, proximal Trp residues dramatically affect PDT-Bimane fluorescence in a distance-dependent manner. This effect is clearly seen in Figure 5, where the Trp residue at site 116 affects the fluorescence intensities of the neighboring PDT-Bimane labels depending on its relative proximity (Table 3, Figure 5B). These observations are consistent with our hypothesis that the Trp quenching is due to photoinduced electron transfer (PET) from Trp to the excited-state bimane (*52*, *53*), since PET is sharply dependent on distance. Formerly, it should be possible to calculate distances between Trp/bimane pairs based on PET transfer rates. However, PET is a complex phenomenon that depends on factors such as solvent polarity (*54*), steric and stereochemical factors (*55*), and the

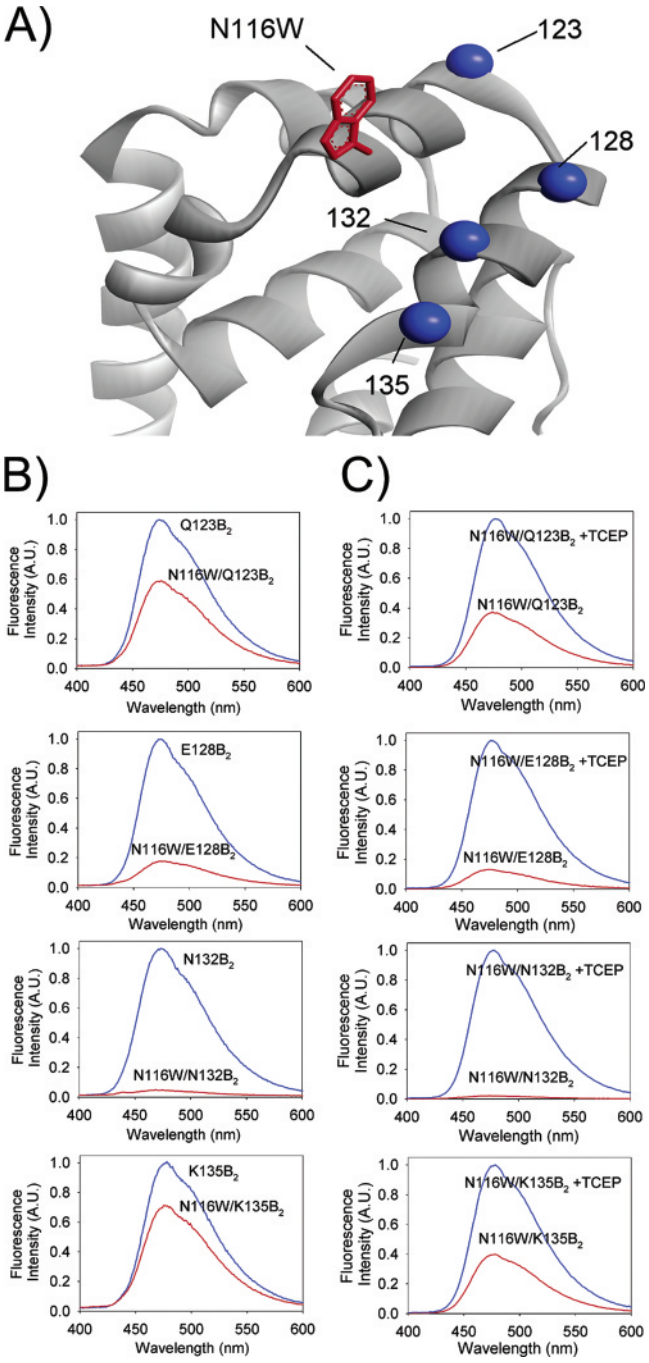

FIGURE 5: PDT-Bimane shows distance-dependent quenching by proximal Trp residues. (A) Model of T4 lysozyme indicating the location of the tryptophan residue and the site of each PDT-Bimane attachment site (the α-carbon sites for each cysteine substitution are shown as blue spheres). (B, left column) Steady-state fluorescence intensity measurements of PDT-Bimane labeled cysteine mutants with (red) and without (blue) the Trp residue at site 116. Notice that introducing the Trp residue at 116 causes a dramatic decrease in fluorescence intensity for labels at sites 128 and 132. (C, right column) Comparison of PDT-Bimane labeled sites with the Trp residue at site 116 before (red) and after (blue) TCEP reduction. Notice that essentially the same results are obtained as in panel B.

relative orientation between the molecule pair (*56*). Thus, quantitative interpretations of distance would require taking these factors into account while also carrying out molecular modeling and analysis of the time-resolved data using a distance-dependent quenching model by Zelent et al. (*57*). Thus, rather than trying to determine distance from PET quenching rates, we have developed a more simple and robust method to assess proximity directly from the fluorescence data, as discussed below.

The degree of Trp/bimane proximity can be determined by assessing the nature of the fluorescence quenching at a given site, by comparing the fluorescence intensity data to the fluorescence lifetime data. Specifically, one compares the ratio of the steady-state fluorescence intensity without and with the presence of the tryptophan residue (F_o/F_w) to the ratio of the weighted fluorescence lifetime data (τ_o/τ_w). From these results, one can determine whether the Trp/bimane pair is "close" and in near contact distance (∼10−15 Å) or "very close" and within contact distance (∼5−10 Å) based on the type of quenching observed; i.e., whether the quenching is dynamic or static in nature.

The rationale for this analysis is as follows: if the Trp/bimane pair is "close", then the quenching can occur through dynamic or collisional mechanisms during the lifetime of the bimane excited state. Such quenching will cause the steady-state fluorescence intensities and the fluorescence lifetimes to decrease by roughly the same amount (thus $F_o/F_w > 1$, $\tau_o/\tau_w > 1$, and $F_o/F_w \approx \tau_o/\tau_w$ (*47*)). In contrast, a special situation is observed for Trp/bimane pairs that are "very close", or within contact distance (∼5−10 Å) at the moment of excitation. For such "very close" pairs, static quenching will occur through the formation of a nonfluorescent ground-state complex and be observed as a drop in fluorescence intensity that is greater than the change seen in the fluorescence lifetime (thus, $F_o/F_w \gg \tau_o/\tau_w$ (*47*)). Note that this type of quenching could also be observed if the quenching occurs faster than the time resolution of our lifetime instrument.

Figure 6 shows an example of how this type of analysis can further resolve Trp/bimane proximity. The data compare the PDT-Bimane labeled sites shown in Figure 5 (123, 128, 132, and 135) with and without the tryptophan residue at site 116. Note that the N116W/E128B$_2$ pair shows substantial steady-state quenching, yet the F_o/F_w and τ_o/τ_w ratios are similar (Figure 6A), indicating the quenching is primarily dynamic, classifying this pair as "close" (∼10−15 Å). In contrast, the lifetime and steady-state ratios do *not* match for mutant N116W/N132B$_2$ (Figure 6A), indicating substantial static quenching, and thus this Trp/bimane pair must be "very close" (∼5−10 Å). These conclusions are consistent with the T4L crystal structure (Figure 5A), and are further supported from an analysis of the absorption spectra, which shows the absorption spectrum for N116W/N132B$_2$ is altered by 6 nm compared to mutant N132B$_2$ alone, further suggesting the Trp residue and bimane label in this pair form a ground-state complex (Figure 6B).

TCEP Reduction Provides a Simple Way to Assess Trp/PDT-Bimane Proximity. Identifying Trp proximity can be determined by comparing quantum yields and fluorescence intensity measurements between carefully matched protein samples (see Figure 5B). However, this process is laborious, and requires measurements be repeated on samples in which the suspected "offending" Trp residue has been mutated to a phenylalanine to relieve the quenching. A similar process is required when using mBBr.

However, the ability to reduce the PDT-Bimane label off the protein dramatically simplifies this process by eliminating

Table 3: Quantum Yields and Lifetime Analysis of the Fluorescence Decay Measurements[a]

mutant	Θ[b]	τ_1 (ns)	α_1	τ_2 (ns)	α_2	χ^2	$\langle\tau\rangle$[c] (ns)
$Q123B_2$	0.097 ± 0.004	6.7 ± 0.3	0.8 ± 0.1	1.4 ± 0.5	0.2 ± 0.1	1.0 ± 0.1	5.6 ± 0.1
$N116W/Q123B_2$	0.059 ± 0.007	5.7 ± 0.2	0.6 ± 0.1	1.3 ± 0.2	0.4 ± 0.1	0.9 ± 0.1	3.9 ± 0.1
$E128B_2$	0.102 ± 0.008	8.5 ± 0.5	0.8 ± 0.1	1.6 ± 0.6	0.2 ± 0.1	0.9 ± 0.1	7.2 ± 0.2
$N116W/E128B_2$	0.019 ± 0.005	5.5 ± 0.1	0.3 ± 0.1	1.0 ± 0.1	0.7 ± 0.1	0.9 ± 0.1	2.5 ± 0.2
$N132B_2$	0.100 ± 0.005	7.0 ± 0.7	0.7 ± 0.1	1.8 ± 0.7	0.3 ± 0.1	1.0 ± 0.1	5.4 ± 0.2
$N116W/N132B_2$	0.006 ± 0.003	6.9 ± 0.2	0.2 ± 0.1	0.5 ± 0.1	0.8 ± 0.1	1.0 ± 0.1	1.7 ± 0.3
$K135B_2$	0.082 ± 0.009	6.2 ± 0.3	0.8 ± 0.1	0.8 ± 0.4	0.2 ± 0.1	1.1 ± 0.1	5.2 ± 0.2
$N116W/K135B_2$	0.059 ± 0.005	5.2 ± 0.2	0.7 ± 0.1	1.3 ± 0.1	0.3 ± 0.1	1.0 ± 0.1	3.9 ± 0.1

[a] Excitation wavelength was 381 nm and emission was collected using two >470 nm long-pass filters. The average of six lifetime measurements $\pm$ the standard error of the mean are reported. Abbreviations: τ_1, τ_2, fluorescence lifetimes in nanoseconds; α_1, α_2, normalized preexponential factors such that $\alpha_1 + \alpha_2 = 1.0$; χ^2, chi-squared value of the fit. [b] The uncertainty reported is the standard deviation from two separate quantum yield measurements. [c] $\langle\tau\rangle = \alpha_1\tau_1 + \alpha_2\tau_2$, the amplitude-weighted fluorescence lifetime. The $\langle\tau\rangle$ values reported in this table represent the average of six sets of lifetimes $\pm$ the standard error of the mean.

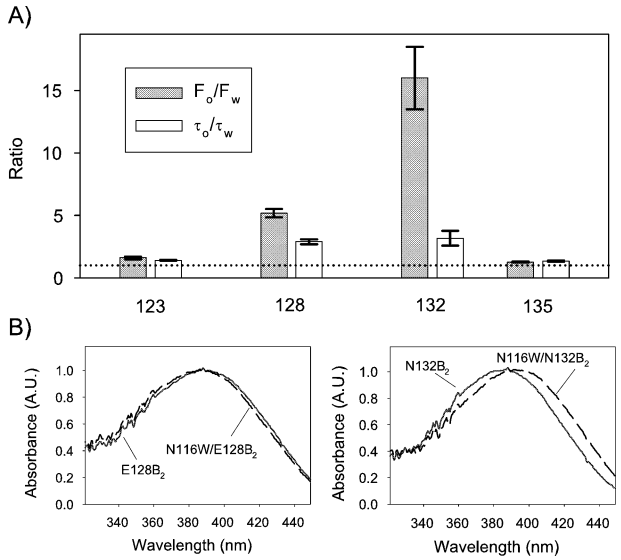

FIGURE 6: Proximity between Trp/bimane pairs can be further resolved by comparing the fluorescence intensities and lifetimes with (F_w; τ_w) and without (F_o; τ_o) a Trp residue. (A) The large difference in the steady-state fluorescence intensity ratio (F_o/F_w) compared to the weighted fluorescence lifetime ratio (τ_o/τ_w) reveals the Trp/bimane pair at $N116W/N132B_2$ undergoes primarily static quenching and thus is "very close" (~5−10 Å), whereas $N116W/E128B_2$ undergoes primarily dynamic quenching and thus is "close" (~10−15 Å). The uncertainty reported is the standard error of the mean from four measurements. (B) Absorption spectra of PDT-Bimane labels at sites 128 and 132 with (dashed line) and without (solid line) the neighboring Trp residue at site 116. The change in the absorption spectra at site 132 suggests a ground-state complex forms for mutant $N116W/N132B_2$, consistent with the static quenching detected in (A).

the need for precisely matching sample concentration or mutating Trp residues. Using PDT-Bimane, the proximity to a nearby tryptophan residue can simply be determined by reducing the label off the protein and assessing the amount of fluorescence increase. Figure 5C shows an example of this approach. Note that some increase in PDT-Bimane fluorescence occurs upon reduction even in the absence of a neighboring Trp residue (possibly due to lesser quenching from other amino acids), and this change explains the limited discrepancy between the data in Figure 5B and Figure 5C. However, as shown in our control experiments in Figure 7, this increase is small compared to the change observed in the presence of a proximal Trp. Reduction of samples not containing neighboring Trp residues ($Q123B_2$, $E128B_2$, $N132B_2$, and $K135B_2$) results in an average 70 $\pm$ 20% increase in fluorescence (Figure 7A), possibly due to relief of quenching by proximal tyrosine residues, which can also quench bimane fluorescence but do so with ~4-fold less efficiency (*58*). In contrast, the fluorescence intensity increase observed after reducing samples that contain a proximal Trp residue are an order of magnitude larger. For example, there is a 600% increase observed for $N116W/E128B_2$ and a 3700% increase for $N116W/N132B_2$ (Figure 7B).

When the inherent ~70% increase in fluorescence intensity caused by TCEP reduction is taken into account, almost identical results are obtained to those using the much more laborious approach of measuring and comparing the quantum yields of samples with and without the Trp residue; compare Figure 7, panel C to D.

These results also suggest the PDT-Bimane reduction method can be used to assess Trp/bimane distances, independent of sample concentration and labeling efficiency. While other powerful methods exist for measuring distances in macromolecules (fluorescence resonance energy transfer (*5*, *9*, *11*, *59*) or spin−spin interactions (*34*, *60*, *61*)), these can sometimes be affected by labeling efficiency and usually require equal concentrations of donor and acceptor. Like these other labeling methods, however, the PDT-Bimane reduction method is sensitive to the amount of contaminating free label, and this must be determined using the methods outlined here.

PDT-Bimane Enables a High Throughput Approach For Assessing Protein Structure and Dynamics. In Figure 8, we outline how PDT-Bimane could be used to simplify and automate SDFL studies. In brief, one would first generate single cysteine protein mutants, label these samples with PDT-Bimane, and determine the amount of labeling and the percent free label in each sample using the TCEP/TCA precipitation protocol. Next, one would determine the extent of solvent exposure at each site by comparing the "apparent polarity" of each bimane label (determined from the emission λ_{max} shifts) before and after TCEP reduction, and use the periodicity in these data to determine the secondary structure of the region under study (in this analysis, sites which do not label would be considered as buried). Finally, the proximity to any Trp residues would be determined by comparing fluorescence intensities before and after TCEP reduction.

At this stage of the analysis, one could deduce both the secondary structure motif of the region being scanned, and which sites are close to Trp residues. However, in proteins of unknown structure, such data would not identify precisely

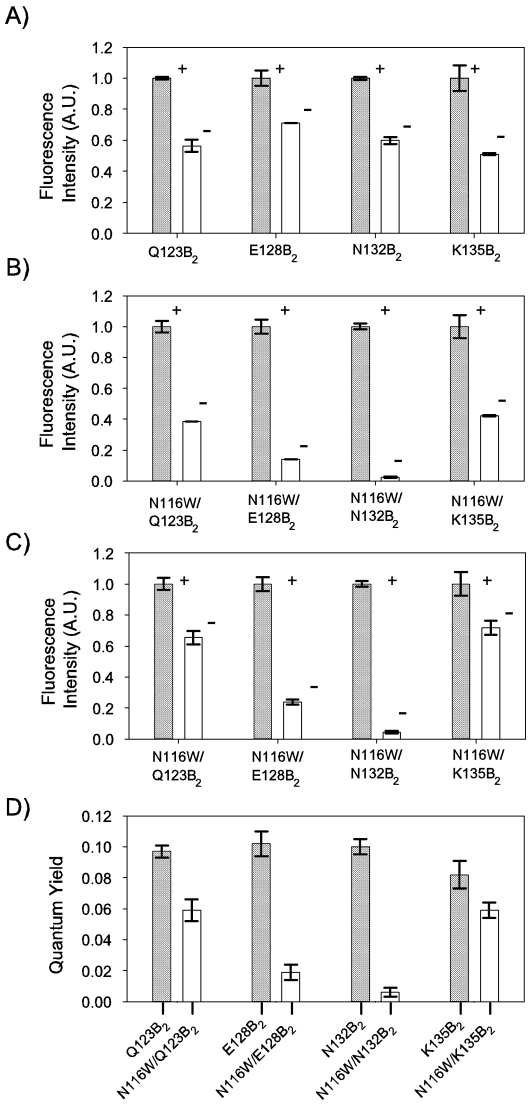

FIGURE 7: Proximity of PDT-Bimane to Trp residues can be determined by simply comparing fluorescence intensity values before and after TCEP reduction. (A) Relative fluorescence intensities of samples $Q123B_2$, $E128B_2$, $N132B_2$, and $K135B_2$ before and after reducing the PDT-Bimane label off the protein with TCEP. Note the inherent increase in bimane fluorescence intensity (~70%) for these samples that do not contain the proximal Trp residue at site 116. (B) The fluorescence intensity increases dramatically upon TCEP reduction of sites with a proximal Trp residue at site 116. (C) Relative fluorescence intensities of samples from (B) after correction for the 70% increase seen in panel A. (D) Quantum yield values of matched concentrations (by absorbance) of the PDT-Bimane labeled samples both with and without the presence of the tryptophan residue at site 116. Note that the data from panel C provides nearly identical values relative to those seen in panel D, yet the TCEP reduction does not require mutating away the Trp residue at site 116 or carefully matching sample concentrations. The uncertainty reported in this figure represent the standard deviation of two measurements.

which tryptophans are next to which bimane labeled sites. To identify these, systematic Trp mutations would still need to be performed, although only for those sites already identified to be affected by Trp residues. Finally, one would classify how close each Trp/bimane pair is by determining if the type of quenching is "dynamic" (10−15 Å) or "static" (5−10 Å), by comparing the fluorescence intensity ratios (F_o/F_w) to the weighted fluorescence lifetime ratios (τ_o/τ_w).

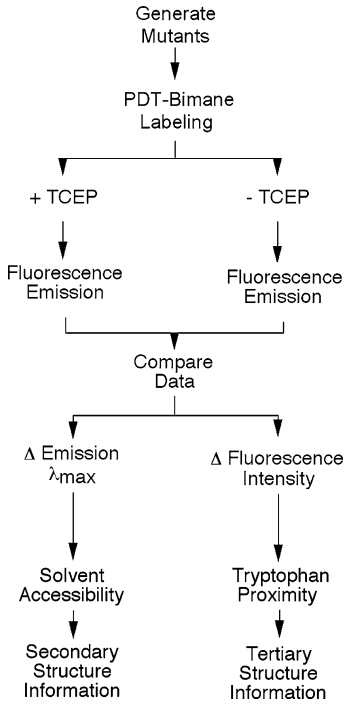

FIGURE 8: Proposed scheme for carrying out high-throughput SDFL studies of protein structure using PDT-Bimane. Briefly, one would label samples with PDT-Bimane and measure fluorescence emission scans with and without TCEP to reduce the label off the protein sample. Comparison of the differences in emission λ_{max} values would reflect the solvent surface accessibility, and thus secondary structure, and the differences in fluorescence intensity values would reflect proximity to tryptophan residues and thus tertiary structure. This approach would lend itself to automation and the use of a fluorescence plate reader, and thus should prove useful for high-throughput protein structural studies.

Conclusions. We have shown PDT-Bimane, like mBBr, can be used in a scanning SDFL approach to determine structural information at the level of the backbone fold and to measure proximity within proteins by the distance-dependent tryptophan quenching method (*3*, *10*). In addition, we demonstrated the ability to reduce PDT-Bimane off the protein can be exploited to (i) quickly and easily quantitate the extent of label incorporation and free label contamination, (ii) assess the extent of solvent exposure of the probe, and (iii) assess label proximity to tryptophan residues. These features of PDT-Bimane make it ideal for use in automated, high-throughput proteomic studies of protein structure and folding, the detection of protein−protein interactions, and the monitoring of protein conformational changes. We also anticipate the unique properties of PDT-Bimane will prove useful for technically challenging studies such as assessing real-time conformational changes in receptors and ion channels in natural membrane environments.

ACKNOWLEDGMENT

We would like to thank our long-standing friend and collaborator at Vanderbilt University, Dr. Hassane McHaourab, for many helpful discussions and a critical reading of this manuscript.

REFERENCES

1. Gether, U., Lin, S., and Kobilka, B. K. (1995) Fluorescent labeling of purified beta 2 adrenergic receptor. Evidence for ligand-specific conformational changes, *J. Biol. Chem. 270*, 28268−28275.

2. Shepard, L. A., Heuck, A. P., Hamman, B. D., Rossjohn, J., Parker, M. W., Ryan, K. R., Johnson, A. E., and Tweten, R. K. (1998) Identification of a membrane-spanning domain of the thiol-activated pore-forming toxin *Clostridium perfringens* perfringolysin O: an alpha-helical to beta-sheet transition identified by fluorescence spectroscopy, *Biochemistry 37*, 14563−14574.
3. Mansoor, S. E., McHaourab, H. S., and Farrens, D. L. (1999) Determination of protein secondary structure and solvent accessibility using site-directed fluorescence labeling. Studies of T4 lysozyme using the fluorescent probe monobromobimane, *Biochemistry 38*, 16383−16393.
4. Glauner, K. S., Mannuzzu, L. M., Gandhi, C. S., and Isacoff, E. Y. (1999) Spectroscopic mapping of voltage sensor movement in the Shaker potassium channel, *Nature 402*, 813−817.
5. Cha, A., Snyder, G. E., Selvin, P. R., and Bezanilla, F. (1999) Atomic scale movement of the voltage-sensing region in a potassium channel measured via spectroscopy, *Nature 402*, 809−813.
6. Dunham, T. D., and Farrens, D. L. (1999) Conformational changes in rhodopsin. Movement of helix f detected by site-specific chemical labeling and fluorescence spectroscopy, *J. Biol. Chem. 274*, 1683−1690.
7. Imamoto, Y., Kataoka, M., Tokunaga, F., and Palczewski, K. (2000) Light-induced conformational changes of rhodopsin probed by fluorescent alexa594 immobilized on the cytoplasmic surface, *Biochemistry 39*, 15225−15233.
8. Ghanouni, P., Steenhuis, J. J., Farrens, D. L., and Kobilka, B. K. (2001) Agonist-induced conformational changes in the G-protein-coupling domain of the beta 2 adrenergic receptor, *Proc. Natl. Acad. Sci. U.S.A. 98*, 5997−6002.
9. Navon, A., Ittah, V., Landsman, P., Scheraga, H. A., and Haas, E. (2001) Distributions of intramolecular distances in the reduced and denatured states of bovine pancreatic ribonuclease A. Folding initiation structures in the C-terminal portions of the reduced protein, *Biochemistry 40*, 105−118.
10. Mansoor, S. E., McHaourab, H. S., and Farrens, D. L. (2002) Mapping proximity within proteins using fluorescence spectroscopy. A study of T4 lysozyme showing that tryptophan residues quench bimane fluorescence, *Biochemistry 41*, 2475−2484.
11. Heyduk, T. (2002) Measuring protein conformational changes by FRET/LRET, *Curr. Opin. Biotechnol. 13*, 292−296.
12. Mielke, T., Alexiev, U., Glasel, M., Otto, H., and Heyn, M. P. (2002) Light-induced changes in the structure and accessibility of the cytoplasmic loops of rhodopsin in the activated MII state, *Biochemistry 41*, 7875−7884.
13. Sathish, H. A., Stein, R. A., Yang, G., and McHaourab, H. S. (2003) Mechanism of chaperone function in small heat-shock proteins. Fluorescence studies of the conformations of T4 lysozyme bound to alphaB-crystallin, *J. Biol. Chem. 278*, 44214−44221.
14. Alexiev, U., Rimke, I., and Pohlmann, T. (2003) Elucidation of the nature of the conformational changes of the EF-interhelical loop in bacteriorhodopsin and of the helix VIII on the cytoplasmic surface of bovine rhodopsin: a time-resolved fluorescence depolarization study, *J. Mol. Biol. 328*, 705−719.
15. Kachel, K., Ren, J., Collier, R. J., and London, E. (1998) Identifying transmembrane states and defining the membrane insertion boundaries of hydrophobic helices in membrane-inserted diphtheria toxin T domain, *J. Biol. Chem. 273*, 22950−22956.
16. Carlsson, K., Osterlund, M., Persson, E., Freskgard, P. O., Carlsson, U., and Svensson, M. (2003) Site-directed fluorescence probing to dissect the calcium-dependent association between soluble tissue factor and factor VIIa domains, *Biochim. Biophys. Acta 1648*, 12−16.
17. O'Neil, K. T., Wolfe, H. R., Jr., Erickson-Viitanen, S., and DeGrado, W. F. (1987) Fluorescence properties of calmodulin-binding peptides reflect alpha-helical periodicity, *Science 236*, 1454−1456.
18. Malenbaum, S. E., Collier, R. J., and London, E. (1998) Membrane topography of the T domain of diphtheria toxin probed with single tryptophan mutants, *Biochemistry 37*, 17915−17922.
19. Chen, Y., and Barkley, M. D. (1998) Toward understanding tryptophan fluorescence in proteins, *Biochemistry 37*, 9976−9982.
20. Gasymov, O. K., Abduragimov, A. R., Yusifov, T. N., and Glasgow, B. J. (2001) Site-directed tryptophan fluorescence reveals the solution structure of tear lipocalin: evidence for features that confer promiscuity in ligand binding, *Biochemistry 40*, 14754−14762.
21. Voss, J., He, M. M., Hubbell, W. L., and Kaback, H. R. (1996) Site-directed spin labeling demonstrates that transmembrane domain XII in the lactose permease of *Escherichia coli* is an alpha-helix, *Biochemistry 35*, 12915−12918.
22. Millhauser, G. L., Fiori, W. R., and Miick, S. M. (1995) Electron spin labels, *Methods Enzymol. 246*, 589−610.
23. Klug, C. S., Su, W., and Feix, J. B. (1997) Mapping of the residues involved in a proposed beta-strand located in the ferric enterobactin receptor FepA using site-directed spin-labeling, *Biochemistry 36*, 13027−13033.
24. Hubbell, W. L., Gross, A., Langen, R., and Lietzow, M. A. (1998) Recent advances in site-directed spin labeling of proteins, *Curr. Opin. Struct. Biol. 8*, 649−656.
25. Perozo, E., Cortes, D. M., and Cuello, L. G. (1998) Three-dimensional architecture and gating mechanism of a K+ channel studied by EPR spectroscopy, *Nat. Struct. Biol. 5*, 459−469.
26. Thomas, D. D., Reddy, L. G., Karim, C. B., Li, M., Cornea, R., Autry, J. M., Jones, L. R., and Stamm, J. (1998) Direct spectroscopic detection of molecular dynamics and interactions of the calcium pump and phospholamban, *Ann. N. Y. Acad. Sci. 853*, 186−194.
27. Hustedt, E. J., and Beth, A. H. (1999) Nitroxide spin−spin interactions: applications to protein structure and dynamics, *Annu. Rev. Biophys. Biomol. Struct. 28*, 129−153.
28. Gross, A., Columbus, L., Hideg, K., Altenbach, C., and Hubbell, W. L. (1999) Structure of the KcsA potassium channel from *Streptomyces lividans*: a site-directed spin labeling study of the second transmembrane segment, *Biochemistry 38*, 10324−10335.
29. Hubbell, W. L., Cafiso, D. S., and Altenbach, C. (2000) Identifying conformational changes with site-directed spin labeling, *Nat. Struct. Biol. 7*, 735−739.
30. Lakshmi, K. V., and Brudvig, G. W. (2001) Pulsed electron paramagnetic resonance methods for macromolecular structure determination, *Curr. Opin. Struct. Biol. 11*, 523−531.
31. Fanucci, G. E., Lee, J. Y., and Cafiso, D. S. (2003) Spectroscopic Evidence that Osmolytes Used in Crystallization Buffers Inhibit a Conformation Change in a Membrane Protein, *Biochemistry 42*, 13106−13112.
32. McHaourab, H. S., Lietzow, M. A., Hideg, K., and Hubbell, W. L. (1996) Motion of spin-labeled side chains in T4 lysozyme. Correlation with protein structure and dynamics, *Biochemistry 35*, 7692−7704.
33. Hubbell, W. L., McHaourab, H. S., Altenbach, C., and Lietzow, M. A. (1996) Watching proteins move using site-directed spin labeling, *Structure 4*, 779−783.
34. McHaourab, H. S., Oh, K. J., Fang, C. J., and Hubbell, W. L. (1997) Conformation of T4 lysozyme in solution. Hinge-bending motion and the substrate-induced conformational transition studied by site-directed spin labeling, *Biochemistry 36*, 307−316.
35. McHaourab, H. S., Kalai, T., Hideg, K., and Hubbell, W. L. (1999) Motion of spin-labeled side chains in T4 lysozyme: effect of side chain structure, *Biochemistry 38*, 2947−2955.
36. Langen, R., Oh, K. J., Cascio, D., and Hubbell, W. L. (2000) Crystal structures of spin labeled T4 lysozyme mutants: implications for the interpretation of EPR spectra in terms of structure, *Biochemistry 39*, 8396−8405.
37. Borbat, P. P., McHaourab, H. S., and Freed, J. H. (2002) Protein structure determination using long-distance constraints from double-quantum coherence ESR: study of T4 lysozyme, *J. Am. Chem. Soc. 124*, 5304−5314.
38. Hosfield, D., Palan, J., Hilgers, M., Scheibe, D., McRee, D. E., and Stevens, R. C. (2003) A fully integrated protein crystallization platform for small-molecule drug discovery, *J. Struct. Biol. 142*, 207−217.
39. Carlsson, J., Drevin, H., and Axen, R. (1978) Protein thiolation and reversible protein−protein conjugation. N-Succinimidyl 3-(2-pyridyldithio)propionate, a new heterobifunctional reagent, *Biochem. J. 173*, 723−737.
40. Becktel, W. J., and Schellman, J. A. (1987) Protein stability curves, *Biopolymers 26*, 1859−1877.
41. James, D. R., Siemiarczuk, A., and Ware, W. R. (1992) Stroboscopic optical boxcar technique for the determination of fluorescence lifetimes, *Rev. Sci. Instrum. 63*, 1710−1716.
42. D'Auria, S., Gryczynski, Z., Gryczynski, I., Rossi, M., and Lakowicz, J. R. (2000) A protein biosensor for lactate, *Anal. Biochem. 283*, 83−88.
43. Hawkins, M. E., Pfleiderer, W., Balis, F. M., Porter, D., and Knutson, J. R. (1997) Fluorescence properties of pteridine nucleoside analogues as monomers and incorporated into oligonucleotides, *Anal. Biochem. 244*, 86−95.

44. Lakowicz, J. R. (1983) *Principles of Fluorescence Spectroscopy*, Plenum Press, New York.
45. Maliwal, B. P., Malicka, J., Gryczynski, I., Gryczynski, Z., and Lakowicz, J. R. (2003) Fluorescence properties of labeled proteins near silver colloid surfaces, *Biopolymers 70*, 585−594.
46. Webber, S. E. (1997) The Role of Time-Dependent Measurements in Elucidating Static Versus Dynamic Quenching Processes, *Photochem. Photobiol. 65*, 33−38.
47. Lakowicz, J. R., and Weber, G. (1973) Quenching of fluorescence by oxygen. A probe for structural fluctuations in macromolecules, *Biochemistry 12*, 4161−4170.
48. Abagyan, R., Totrov, M., and Kuznetsov, D. N. (1994) ICM − a new method for protein modelling and design. Applications to docking and structure prediction from the distorted native conformation, *J. Comput. Chem. 15*, 488−506.
49. Nicholson, H., Anderson, D. E., Dao-pin, S., and Matthews, B. W. (1991) Analysis of the interaction between charged side chains and the alpha-helix dipole using designed thermostable mutants of phage T4 lysozyme, *Biochemistry 30*, 9816−9828.
50. Han, J. C., and Han, G. Y. (1994) A procedure for quantitative determination of tris(2-carboxyethyl)phosphine, an odorless reducing agent more stable and effective than dithiothreitol, *Anal. Biochem. 220*, 5−10.
51. Hu, L., and Colman, R. F. (1995) Monobromobimane as an affinity label of the xenobiotic binding site of rat glutathione S-transferase 3−3, *J. Biol. Chem. 270*, 21875−21883.
52. Kosower, E. M., Giniger, R., Radkowsky, A., Hebel, D., and Shusterman, A. (1986) Bimanes 22. Flexible fluorescent molecules. Solvent effects on the photophysical properties of syn-bimanes (1,5-diazabicyclo[3.3.0]octa-3,6-diene-2,8-diones), *J. Phys. Chem. 90*, 5552−5557.
53. Kosower, E. M., Kanety, H., Dodluk, H., and Hermolin, J. (1982) Bimanes. 9. Solvent and substituent effects on intramolecular charge-transfer quenching of the fluorescence of syn-1,5-diazabicyclo[3.3.0]octadienediones (syn-9,10-dioxabimanes), *J. Phys. Chem. 86*, 1270−1277.
54. Lockhart, D. J., and Kim, P. S. (1992) Internal stark effect measurement of the electric field at the amino terminus of an alpha helix, *Science 257*, 947−951.
55. Closs, G. L., and Miller, J. R. (1988) Intramolecular Long-Distance Electron Transfer in Organic Molecules, *Science 240*, 440−447.
56. Siders, P., Cave, R. J., and Marcus, R. A. (1984) A model for orientation effects in electron-transfer reactions, *J. Chem. Phys. 81*, 5613−5624.
57. Zelent, B., Kusba, J., Gryczynski, I., Johnson, M. L., and Lakowicz, J. R. (1998) Time-resolved and steady-state fluorescence quenching of *N*-acetyl-L-tryptophanamide by acrylamide and iodide, *Biophys. Chem. 73*, 53−75.
58. Sato, E., Sakashita, M., Kanaoka, Y., and Kosower, E. M. (1988) *Bioorg. Chem. 16*, 298−306.
59. Heyduk, T., and Heyduk, E. (2002) Molecular beacons for detecting DNA binding proteins, *Nat. Biotechnol. 20*, 171−176.
60. Farrens, D. L., Altenbach, C., Yang, K., Hubbell, W. L., and Khorana, H. G. (1996) Requirement of rigid-body motion of transmembrane helices for light activation of rhodopsin, *Science 274*, 768−770.
61. Liu, Y. S., Sompornpisut, P., and Perozo, E. (2001) Structure of the KcsA channel intracellular gate in the open state, *Nat. Struct. Biol. 8*, 883−887.

BI036259M